On the role of membrane anisotropy and BAR proteins in the stability of tubular membrane structures

Doron Kabaso [a,*], Nataliya Bobrovska [a,d], Wojciech Góźdź [d], Nir Gov [e], Veronika Kralj-Iglič [b], Peter Veranič [c], Aleš Iglič [a]

[a] Laboratory of Biophysics, Faculty of Electrical Engineering, University of Ljubljana, Ljubljana, Slovenia
[b] Laboratory of Clinical Biophysics, Faculty of Medicine, University of Ljubljana, Ljubljana, Slovenia
[c] Institute of Cell Biology, Faculty of Medicine, University of Ljubljana, Ljubljana, Slovenia
[d] Institute of Physical Chemistry, Polish Academy of Sciences, Warsaw, Poland
[e] Department of Chemical Physics, Weizmann Institute of Science, Rehovot, Israel

ARTICLE INFO

ABSTRACT

Recent studies have demonstrated that actin filaments are not crucial for the short-term stability of tubular membrane protrusions originating from the cell surface. It has also been demonstrated that prominin nanodomains and curvature inducing I-BAR proteins could account for the stability of the membrane protrusion. Here we constructed an axisymmetric model of a membrane protrusion that excludes actin filaments in order to investigate the contributions of prominin nanodomains (rafts) and I-BAR proteins to the membrane protrusion stability. It was demonstrated that prominin nanodomains and I-BAR proteins can stabilize the membrane protrusion only over a specific range of spontaneous curvature. On the other hand, high spontaneous curvature and/or high density of I-BAR proteins could lead to system instability and to non-uniform contraction in the radial direction of the membrane protrusion. In agreement with previous studies, it was also shown that the isotropic bending energy of lipids is not sufficient to explain the stability of the observed tubular membrane protrusion without actin filaments.

1. Introduction

Cell membrane structures with tubular geometry include various cellular shapes such as filopodia, microvilli and membrane nanotubes (Weigmann et al., 1997; Corbeil et al., 2001; Mattila et al., 2007; Gerdes et al., 2007; Veranič et al., 2008; Davis and Sowinski, 2008; Hurtig et al., 2010; Lokar et al., 2010; Dubey and Ben-Yehuda, 2011). In bilayer membrane systems, lipid–lipid and lipid–protein direct interactions may result in formation of small membrane (in general anisotropic) nanodomains (clusters, inclusions), which can stabilize the tubular membrane protrusion and contribute to lipid and protein sorting (Iglič et al., 2006; Tian and Baumgart, 2009; Sorre et al., 2009; Góźdź, 2011). Without the application of direct mechanical force, tubular membrane budding may be explained by accumulation and in-plane average ordering of anisotropic membrane nanodomains in tubular membrane protrusions (Iglič et al., 2006; Gimsa et al., 2007; Janich and Corbeil, 2007; Hurtig et al., 2010), where the difference between the two principal membrane curvatures C_1 and C_2 is very large

(Iglič et al., 2007a; Tian and Baumgart, 2009; Sorre et al., 2009; Jorgačevski et al., 2010; Risselada et al., 2011). On the other hand, the isotropic bilayer elasticity is not sufficient to overcome the loss of configurational (mixing) entropy due to the sorting of lipids between the tubular membrane protrusion and the parent membrane (Iglič et al., 2006; Tian and Baumgart, 2009).

In cellular systems, it was shown that intracellular actin filaments and membrane components such as prominin nanodomain rafts and I-BAR proteins could stabilize and facilitate the growth of the membrane protrusion (Weigmann et al., 1997; Corbeil et al., 2001; Mattila et al., 2007; Zhao et al., 2010; Hurtig et al., 2010). Demonstrating the importance of the membrane components alone, the membrane protrusion remained stable following the degradation of the inner rod cytoskeleton, presumably due to the residual anisotropic membrane components (Iglič et al., 2006; Veranič et al., 2008). In a different study, it has been shown that the polymerization of actin filaments lagged behind the accumulation of I-BAR proteins at the growing tip of the membrane protrusion, suggesting that actin polymerization is less crucial for the growth of membrane protrusions than believed in the past (Yang et al., 2009). Interestingly, the tubular membrane protrusions that lacked actin filaments had irregular shapes of non-uniform diameter. Thus, the underlying mechanisms responsible

---

for the stability and shape of the tubular membrane protrusion still partially remain a puzzling question. In this theoretical study, we hypothesize that the intrinsic (spontaneous) curvature of anisotropic nanodomain rafts (e.g. prominin rafts) stabilize the membrane protrusion, while the high density of BAR (e.g. I-BAR) proteins accounts for the contraction of the tubular structure, leading to irregularities in the diameter distribution of the membrane protrusion.

Specific raft formations have been indicated on highly curved tubular membrane protrusions (Corbeil et al., 2001; Janich and Corbeil, 2007; Hurtig et al., 2010). These rafts differ from rafts in the plane regions of the plasma membrane (Weigmann et al., 1997). It was shown that at subcellular level (irrespective of the cell type), the membrane protein prominin is preferentially localized in microvilli of epithelial cells and in some other plasma membrane protrusions (Weigmann et al., 1997; Huttner and Zimmerberg, 2001). To exemplify the information content of prominin proteins, the transfection of prominin proteins in mammalian CHO cells lead to their localization in membrane protrusions such as filopodia, lamellipodia and microspikes (Weigmann et al., 1997). The protein prominin was also found to interact directly with plasma membrane cholesterol in cholesterol-based membrane nanodomains (Röper et al., 2000). Thus, the notation of prominin nanodomain rafts in the present study can be replaced by cholesterol-based microdomains, which have also been suggested to be responsible for the stability of highly curved structures (Jorgačevski et al., 2010; Rituper et al., 2010).

I-BAR domains belong to the large family of BAR (Bin/Amphiphysin/Rvs) domains, which can either stabilize or induce different membrane curvatures (Mattila et al., 2007; Scita et al., 2008; Saarikangas et al., 2009, for a review see Kabaso et al., 2011b). In contrast to other family members of the BAR proteins that induce invaginations (Rustom et al., 2004; Itoh et al., 2005; Shimada et al., 2007; Heath and Install, 2008), the I-BAR domains induce membrane protrusions (Millard et al., 2005; Mattila et al., 2007; Scita et al., 2008; Saarikangas et al., 2009). The I-BAR domain could bend the lipid bilayer by electrostatic attraction between the positively charged amino acids and the negatively charged lipids. The overexpression of different I-BAR domains in GUVs caused the formation of membrane tubules of different diameters ranging from 40 nm to 60 nm (Saarikangas et al., 2009). While the present paper focuses on I-BAR proteins, the same theoretical model could be applied to explain the stability and shape of other tubular structures such as the membrane invaginations induced by the binding of N-BAR proteins to the lipid bilayer (Rustom et al., 2004; Itoh et al., 2005; Shimada et al., 2007).

Previous theoretical studies have shown that coupling between the intrinsic (spontaneous) curvature of BAR proteins and the membrane curvature would cause instability, leading to the growth and coalescence of membrane protrusions (Veksler and Gov, 2007; Kabaso et al., 2011a), as well as the division of cells (Shlomovitz and Gov, 2008). In this work we extend the expression for the membrane bending free energy by including the deviatoric energy of anisotropic prominin nanodomains (Iglič et al., 2006; Gimsa et al., 2007; Hurtig et al., 2010) and by coupling the spontaneous curvature of I-BARs with the membrane curvature. The phase separation of anisotropic prominin nanodomains, i.e. their accumulation in tubular membrane protrusion, is elucidated theoretically.

2. Curvature induced segregation of isotropic and anisotropic membrane nanodomains

We investigated two-component (A and B) axisymmetric closed bilayer vesicles, where the components were characterized by different intrinsic (spontaneous) curvatures. We considered two models where the first (A) component was either isotropic or anisotropic. The free energy of the anisotropic membrane can be written in the form (Fischer, 1992; Kralj-Iglič et al., 1999; Iglič et al., 2005; Fošnarič et al., 2006; Iglič et al., 2006)

$$F = \int (\kappa[(H-H_m(\phi))^2 + (D-D_m(\phi))^2]$$
$$+ \frac{kT}{a_0}[\phi \ln(\phi) + (1-\phi) \ln(1-\phi)]) \, dA, \tag{1}$$

where κ is the membrane elastic constant, $H = (C_1+C_2)/2$ is the local membrane mean curvature, $D = |(C_1-C_2)/2|$ is the local membrane curvature deviator, where C_1 and C_2 are the two principal curvatures, $H_m = (C_{1m}+C_{2m})/2$ is the intrinsic (spontaneous) membrane mean curvature, $D_m = |(C_{1m}-C_{2m})/2|$ is the intrinsic (spontaneous) membrane curvature deviator (see Fig. 1), and C_{1m} and C_{2m} are the intrinsic (spontaneous) membrane principal curvatures. The last term in Eq. (1) is the configurational entropy of nanodomains of component A (see also Supplementary Material), where a_0 is the area per single nanodomain of type A, ϕ is the local relative concentration of nanodomains of type A, k is the Boltzmann constant, and T is the temperature. The integral is taken over the surface of the vesicle. The intrinsic (spontaneous) mean and deviatoric membrane curvatures depend on the relative local concentration of type A membrane nanodomains (ϕ) in the following way: $H_m(\phi) = (H_m^A - H_m^B)\phi + H_m^B$ and $D_m(\phi) = (D_m^A - D_m^B)\phi + D_m^B$, where H_m^A and H_m^B are the spontaneous (intrinsic) mean curvatures of components A and B respectively, and D_m^A and D_m^B are the spontaneous (intrinsic) curvature deviators of membrane components A and B, respectively.

In the limit of the isotropic membrane when $D_m = 0$, i.e. $C_{1m} = C_{2m}$ (see Fig. 1), Eq. (1) transforms into the Helfrich expression for the membrane bending energy (first two terms of the equation) (Helfrich, 1973)

$$F = \int \left(\frac{\kappa}{2}(2H-C_0(\phi))^2 + \kappa_G C_1 C_2 \right.$$
$$\left. + \frac{kT}{a_0}[\phi \ln(\phi) + (1-\phi) \ln(1-\phi)] \right) dA, \tag{2}$$

where the constant term $H_m^2/2$ was neglected. Here the Helfrich spontaneous curvature $C_0(\phi) = H_m(\phi) = C_{1m}(\phi) = C_{2m}(\phi)$, κ_G is the saddle-splay (Gaussian) local bending constant (see also Iglič et al., 2005, 2007a,b). In the following the Gaussian term is neglected, since it is constant for the given membrane topology.

We minimized the functional (1) and (2) for two-component vesicles with axisymmetric shapes under the constraints of constant reduced volume v and a global concentration of type A nanodomains $\phi_{tot} = \int \phi \, dA$. The reduced volume is the ratio of the volume of the vesicle to the volume of a sphere with the same

A	B	C	D
$H_m > 0, D_m = 0$	$H_m = D_m = 0$	$H_m = D_m$	$H_m = 0, D_m > 0$
$C_{1m} = C_{2m} > 0$	$C_{1m} = C_{2m} = 0$	$C_{1m} > 0$ $C_{2m} = 0$	$C_{1m} > 0$ $C_{2m} < 0$
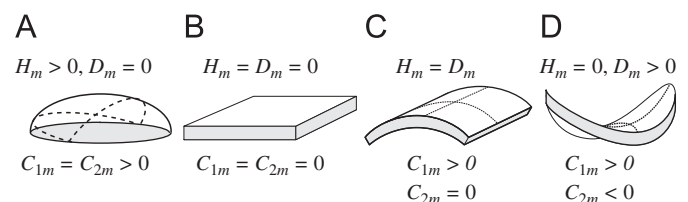
Fig. 1. A schematic figure of the most favourable shapes of a small part of a membrane (membrane nanodomain) having different values of the intrinsic mean curvature (H_m) and intrinsic curvature deviator (D_m). The small part of the membrane may have spherical (A), plane (B), cylindrical (C) or saddle-like (D) intrinsic curvatures. The spherical and plane intrinsic shapes are considered to be isotropic ($D_m = 0$), while the cylindrical and saddle-like intrinsic shapes are considered to be anisotropic ($D_m > 0$). Note that C_{1m} and C_{2m} are the intrinsic (spontaneous) membrane curvatures.

surface area as the given vesicle. The calculations were performed for $\phi_{tot} = 0.5$ and $H_M^A = 8$, $H_M^B = 0$, and several different values of the reduced volume. For the anisotropic case, the spontaneous curvature deviators were $D_m^A = 2.0$ and $D_m^B = 0$, respectively. The bending constant was $\kappa = 30$ kT and $a_0 = 1/600$ where the unit length was set by the radius of a spherical cell (vesicle) with the same surface area as the investigated vesicle R. The value of a_0 corresponds to a vesicle with radius of the order of 250 nm and surface area of the nanodomains of the order of 100 nm^2. The vesicle shape was parametrized by the angle which forms the tangent to the shape profile with the rotational axis as a function of the arclength s (Góźdź, 2004, 2005, 2006). The relative concentration of type A nanodomains was parametrized by the function $\phi(s) = \frac{1}{2}(\phi^A - \phi^B)[1 - \tanh(\xi(s - s_0))] + \phi^B$, where s_0 is the position of the boundary between the region rich in component A and the region rich in component B, ξ is the slope of the concentration profile at s_0. ϕ^A and ϕ^B are the concentrations in the regions rich in components A and B, respectively.

Fig. 2 presents the predicted membrane protrusion shape (calculated as described in online Supplementary Materials) of the isotropic (upper panel) and anisotropic (two lower panels) cases. We showed that a system composed of anisotropic and
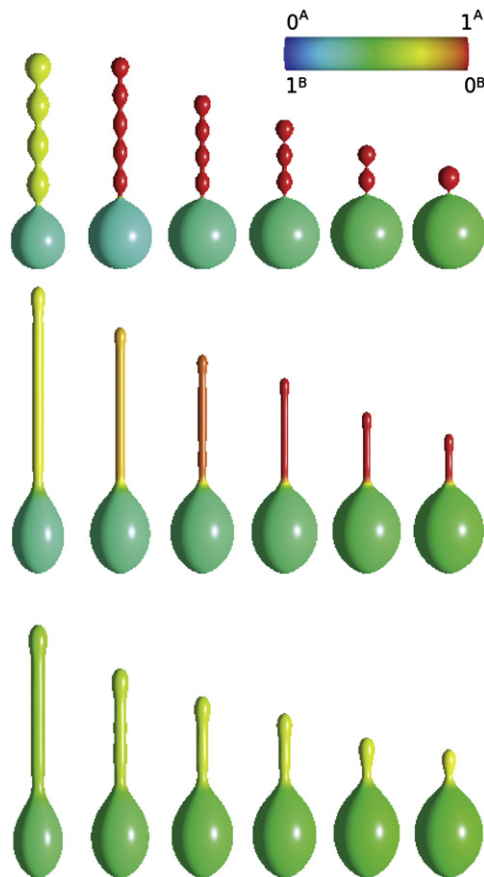
Fig. 2. Comparison of the shapes of two component vesicles calculated for different reduced volume for the isotropic and anisotropic models. The first two rows show the shapes of the vesicles when the entropy contribution is neglected. In the first row, the shapes of the vesicles calculated for the isotropic model with $H_m^A = 8$, $H_m^B = 0$, $D_m^A = 0$, $D_m^B = 0$ are presented. In the second and third row, the shapes of the vesicles calculated for the anisotropic model with $H_m^A = 8$, $H_m^B = 0$, $D_m^A = 2.0$, $D_m^B = 0$ are shown. The calculations in the third row were performed for $\kappa = 30$ kT and $a_0 = 1/600$, where the radius of the vesicle R is the unit of length. The values of reduced volume are (from left to right) $v = 0.54$, 0.67, 0.75, 0.80, 0.85, 0.90, $\phi = 0.5$. The colour of the surface represents the concentration of the components according to the colour map located at the top. (For interpretation of the references to colour in this figure legend, the reader is referred to the web version of this article.)

isotropic components favours the formation of a tubular membrane protrusion, whereas a system composed of only the isotropic components can only form necklace-like membrane protrusions. The deviatoric energy of the anisotropic component attains its minimum upon partial accumulation of the anisotropic component in the tubular protrusion. The driving force for the segregation of isotropic components is solely from the mismatch between the spontaneous curvature of the isotropic component and the membrane curvature.

It can also be seen in Fig. 2 that taking into account the contribution coming from the entropy of mixing does not destroy the cylindrical shape of the protrusions for the anisotropic model. Therefore, the model system considered in the following section is the membrane protrusion without the parent membrane, and the inner membrane component is only of the anisotropic type. Further, we investigated the added effect of attached (outer membrane) I-BAR proteins on the stability of the membrane protrusion.

3. The dynamic model

In this section we considered only a membrane protrusion which is not attached to the parent cell, i.e. we studied axisymmetric myelin (tubular) membrane shapes with an anisotropic membrane (Fig. 3). The membrane undulations were considered in the radial direction ($r(z)$), where z is the axisymmetric axis of the membrane protrusion. The membrane free energy was derived for a system that includes anisotropic prominin nanodomain rafts and attached anisotropic I-BAR proteins (Fig. 3). The anisotropic prominin nanodomains are part of a tubular aggregate of lipids and proteins (Iglič et al., 2006; Hurtig et al., 2010), assumed to be homogeneously distributed along the protrusion (Iglič et al., 2006; Gimsa et al., 2007) in accordance with the results presented in the previous section (Fig. 2). On the other hand, the density of I-BAR proteins is assumed to be non-evenly distributed (Fig. 3). The equations of membrane motion (shape undulations) and the density of I-BARs were derived from differentiation of the membrane free energy. The equations of motion were then linearised. The interaction matrix was obtained from the linearised equations. The equilibrium radius of the membrane protrusion was analysed in the limit of anisotropic and isotropic prominin nanodomains (rafts). Phase diagrams were constructed to reveal the interplay between the prominin nanodomain rafts and I-BAR proteins, as well as the effects of I-BAR protein density on the stability of the membrane protrusion. For details of the definitions of the membrane curvatures and the derivation of the membrane free energy of isotropic and anisotropic elastic properties, see online Supplementary Material.

3.1. Addition of I-BAR proteins

We next considered the addition of I-BAR proteins as an outer membrane component (Fig. 3). Due to curvature-dependent fluxes (Kabaso et al., 2010), the lateral density of I-BARs is predicted to aggregate in regions of favourable (positive) membrane curvature, while being depleted from regions of unfavourable (negative) membrane curvature (Perutkova et al., 2010). The elastic curvature energy of a single I-BAR protein attached to the inner membrane surface is (Perutkova et al., 2010; Baumgart et al., 2011)

$$E_p = \frac{\kappa_p L_0}{2}(C - C_p)^2, \tag{3}$$

where κ_p and L_0 are the flexural rigidity and length of the protein, respectively, C_p is the intrinsic (spontaneous) curvature of I-BAR
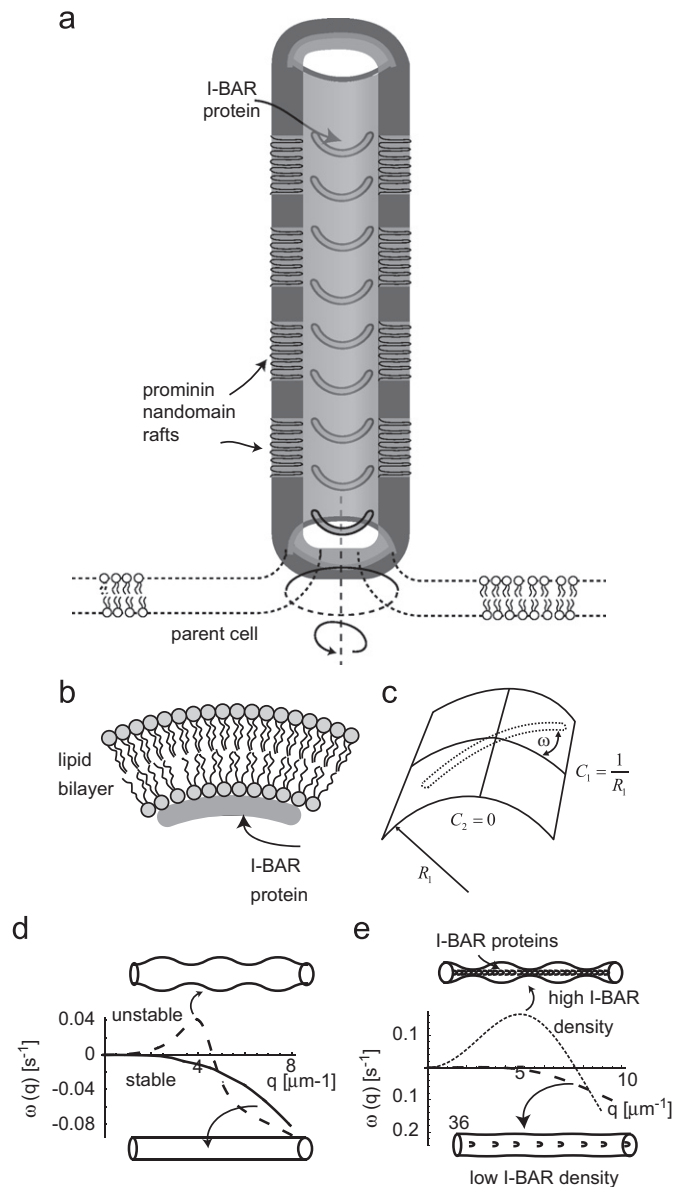
Fig. 3. (a) Schematic diagram of the underlying mechanisms responsible for the stability of the membrane protrusion. The membrane protrusion is considered as a tubular aggregate (Iglič et al., 2006; Gimsa et al., 2007; Hurtig et al., 2010) of anisotropic or isotropic prominin nanodomains. (b) The mobile I-BAR proteins of anisotropic spontaneous curvature lie in a direction perpendicular to the major axis of the tube. (c) Schematic diagram of a flexible rod-like protein strongly attached to the inner side of a cylindrical membrane surface. The principal curvatures of the outer surface are $C_1 = 1/R_1$ and $C_2 = 0$, i.e. $H = D = 1/R_1$. At a given value of the protein orientation angle ω the protein senses the curvature $C = (C_1+C_2)/2 + ((C_1-C_2)/2) \cos(2\omega)$ (adapted from Perutkova et al., 2010). (d) The dispersion relations arising from the linear stability analysis reveal that the membrane of anisotropic (bold line) elastic properties is stable, whereas the isotropic (dashed line) counterpart is unstable. Note that the eigenvector $\omega(q)$ is plotted for different modes q, and that the positive and negative values of $\omega(q)$ describe unstable and stable regions, respectively. (e) The effects of low I-BAR density ($n=0.1$; dashed line) and high I-BAR density ($n=1$; dotted line) on the system stability are evaluated. Note that for large I-BAR density the membrane becomes more undulating.

proteins, and $C = H + D \cos(2\omega)$ is the membrane curvature seen by the I-BAR at the rotational angle ω between the normal plane in which the protein is lying and the plane of the first principal curvature C_1 (along the radial direction). The mean local membrane curvature (H) and membrane curvature deviator (D) were defined before. Due to the assumption $C_p \geq C$ for all ω, the I-BAR protein is oriented in the direction perpendicular ($\omega = 0$) to the major axis of the protrusion (Fig. 3), and as a result, $C = C_1$. The

added contribution of I-BARs to the membrane free energy density (Eqs. (1) and (2)) is

$$F_p = \frac{\eta n_s}{2}(C_1 - C_p)^2 n, \tag{4}$$

where n is the uniform relative density of I-BARs, $\eta = \kappa_p L_0$, and n_s is the saturation area density of I-BARs (Kabaso et al., 2011b). In order to avoid high lateral densities of I-BAR proteins, we considered the excluded volume principle, i.e. the finite volume of I-BARs, by the application of lattice statistics. The details of the lattice statistics employed and the derivation of the system free energy are given in the online Supplementary Material.

3.2. Linear stability analysis

In the following linear stability analysis, the entropy term was neglected for the sake of simplicity. The equations of membrane motion were first derived from differentiation of the free energy. These equations were then linearised. From the linear part, we studied the effects of each parameter on the equilibrium radius of the membrane protrusion. The interaction matrix between prominin nanodomain rafts and I-BAR proteins was obtained by taking the coefficient of the amplitude (i.e. small deviation) $h(z)$, or the I-BAR density $n(z)$, from the equations of motion of membrane height deflection and of I-BAR density, respectively.

The equation of motion of the membrane height deflection along the cylindrical main axis is given by

$$\varphi \frac{\partial h(z)}{\partial t} = -\frac{\partial F_i}{\partial h(z)}, \quad i = iso, \; aniso, \tag{5}$$

where φ is the coefficient of friction describing the drag of the fluid surrounding the membrane, t is the time, and F_i is the free energy of the isotropic or anisotropic case.

The equation of motion of the I-BAR proteins is

$$\frac{\partial n(z)}{\partial t} = \frac{\Lambda}{n_s} \frac{\partial}{\partial z}\left(n(z)\frac{\partial}{\partial z}\frac{\partial F_i}{\partial n(z)}\right), \tag{6}$$

where Λ is the mobility of I-BARs in the membrane and n_s is the saturation density. Note that the normal diffusion term $D_f \partial^2 n(z)/\partial z^2$ is included in the first term on the right hand side of Eq. (6), and that $\Lambda = D_f/kT$, where D_f is the diffusion coefficient of I-BARs.

We next performed stability analysis for a membrane that contains uniformly anisotropic or isotropic curved components, in addition to mobile I-BAR proteins. The tubular membrane was considered to be infinitely long. By a small perturbation to the uniform initial state, we obtained

$$r(z) = R + \delta h(z,t),$$

$$n(z) = \frac{N_t}{n_s R} + \delta n(z,t), \tag{7}$$

where R is the uniform steady state radius of the membrane protrusion, and N_t is the total number of I-BAR proteins per unit length, such that $N_t/n_s R$ is the initial relative density that depends on the membrane protrusion radius R, $\delta h(z,t)$ and $\delta n(z,t)$ are small deviations from the corresponding uniform values. Note that the relative density of I-BARs is unitless (i.e. it is given in terms of fractional area coverage).

The linearisation of Eqs. (5) and (6) yields

$$\varphi \frac{\partial h(z)}{\partial t} = \int (U + \delta L(h,n) + O(\delta^2))\, dA, \tag{8}$$

$$\frac{\partial n(z)}{\partial t} = \delta N(h,n) + O(\delta^2), \tag{9}$$

where the functions $\delta L(h,n)$ and $\delta N(h,n)$ describe the small undulation in the membrane forces and the intra-membrane fluxes, respectively. The forces acting on the membrane in the

equilibrium state are described by U, which is not a function of $h(z)$ or $n(z)$. More details of the linear stability analysis employed are given in the online Supplementary Material.

The solution to the determinant of the stability matrix obtained from the linear stability analysis gives two eigenvectors ($\omega(q)$). The first eigenvector is negative, while the second eigenvector can be positive or negative. The plot of the eigenvector $\omega(q)$ as a function of q is a dispersion relation. In this dispersion relation, the positive regions ($\omega(q) > 0$) describe regions of unstable contraction leading to the formation of tubular dilations, while negative regions ($\omega(q) < 0$) describe stable regions, characterized by the decay of an initial perturbation (Fig. 3). By comparing the dispersion relations of the isotropic and anisotropic cases, the role of prominin nanodomains and I-BAR proteins on the stability of the system could be investigated (Fig. 5). The effect of prominin anisotropy on the system instability was also evaluated.

4. Results

4.1. Equilibrium radius

We set out to analyse the effects of varying each of the parameters in the free energies of the anisotropic and isotropic cases on the equilibrium radius (R_{eq}). The spontaneous mean curvature of the tubular aggregate of prominin nanodomains is H_P, the intrinsic (spontaneous) curvature of the I-BAR protein is C_p, the surface tension coefficient is σ, the elastic membrane constant of the tubular aggregate is κ, and η is proportional to the I-BAR flexural rigidity. The parameter values used for the analysis were as follows: $N_t = 0.1\ \mu m^{-1}$, $n_s = 10\ \mu m^{-2}$, $H_P = 4\ \mu m^{-1}$, $C_p = 70\ \mu m^{-1}$, $\sigma = 0.001\ g\ s^{-2}$, $\kappa = 100\ kT$, $\eta = 1\ kT$, $\varphi = 125\ g\ s^{-1}$. The spontaneous curvatures of prominin nanodomain rafts and I-BAR proteins were set according to the experimental radius of curvature of membrane protrusions and derived tubules from GUVs (Saarikangas et al., 2009). The contributions of I-BAR proteins to the bending modulus (i.e. $\eta n_s/2$) were assumed to be smaller than the elastic constant of the tubular aggregate of prominin nanodomains. The initial uniform relative density $N_t/(n_s R)$ for the given set of parameters gave an approximate initial value of 0.07. Incorporating the above parameter values into R_{eq} gave for the isotropic and anisotropic cases an equilibrium radius of 0.16 μm and 0.12 μm, respectively. Fig. 4 shows the effects of varying the spontaneous curvature of prominin nanodomains (H_P), the spontaneous curvature of I-BARs (C_p), the total number of I-BARs per unit length (N_t), the membrane surface tension (σ), the bending modulus of the tubular membrane with prominin nanodomains (κ), and the flexural coefficient of I-BARs (η), on the equilibrium radius of the isotropic (bold lines) and
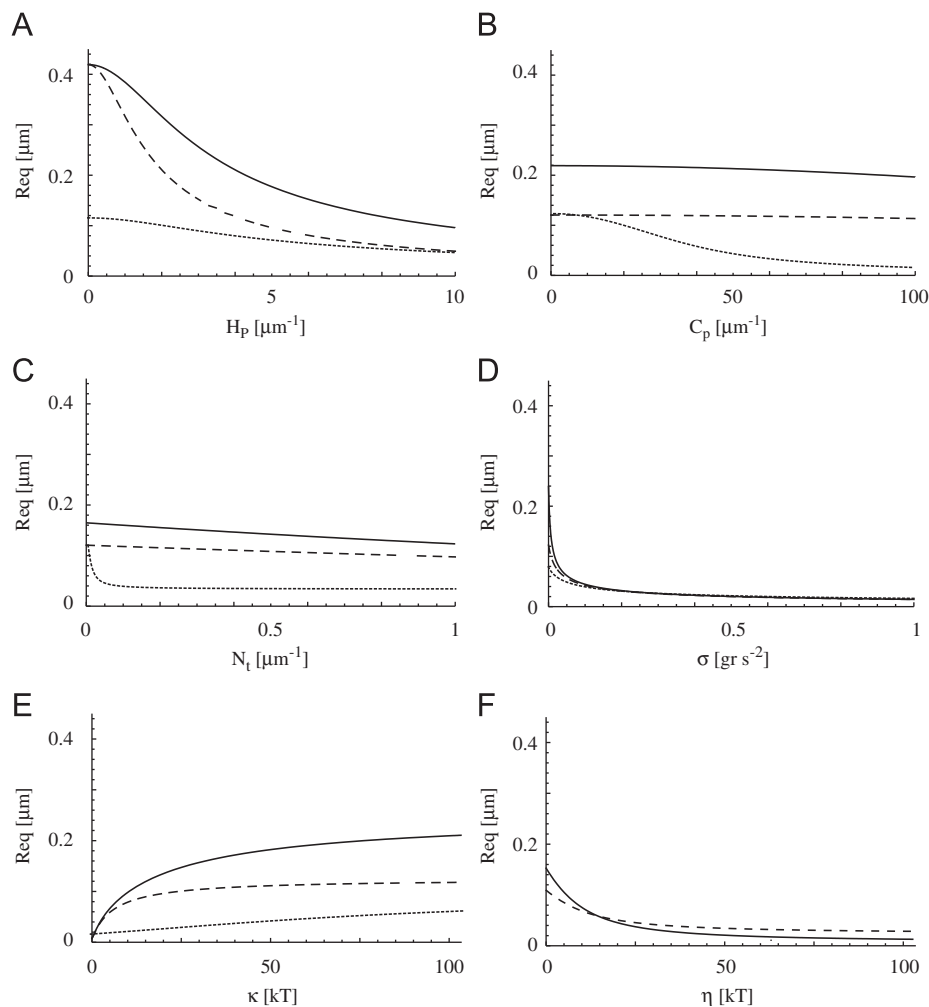
Fig. 4. Effects of varying the different system parameters on the equilibrium tube radius (R_{eq}). The effects of varying the spontaneous curvature of prominin nanodomains (A), the spontaneous curvature of I-BARs (B), the total number of I-BARs (C), the surface tension (D), the elastic constant of prominin nanodomains (E), and the flexural coefficient of I-BARs (F), on the equilibrium radius (R_{eq}) for a tubular membrane with isotropic (bold lines) and anisotropic (dashed lines) elastic properties. The effects of large η (dotted lines) are analysed for a tubular membrane of anisotropic elastic properties. Note that the spontaneous mean curvature of prominin nanodomains (H_P) has the largest effect on R_{eq} (A), and that I-BARs have a large effect on R_{eq} only when the flexural coefficient η is of the same order as κ.

anisotropic (dashed lines) cases. In addition, the case of large η was also analysed for each of the parameters (dotted lines). It was shown that the equilibrium radius of the anisotropic case was always smaller than its isotropic counterpart. In addition, large values of H_P reduced the equilibrium radius. The effects of C_p and N_t depended on the flexural coefficient (η), such that for small η their effect was negligible, whereas for large η (i.e. of the same scale as κ) the effect became considerable (Fig. 4).

4.2. Phase diagrams

Phase diagrams were drawn in order to reveal the interplay between prominin nanodomains and I-BAR proteins. The solution of the stability matrix M was obtained from its determinant. The terms of the determinant were collected according to their order in q as follows:

$$[\lambda_1, \lambda_2] = q^2(q^4 A + q^2 B + C), \tag{10}$$

where the coefficients A, B, and C are functions of the different physical parameters (for details of the coefficient functions see online Supplementary Material), λ_1 and λ_2 are the two possible solutions of the quadratic equation $r^2 A + rB + C$, where $r = q^2$. At the transition between instability and stability, the roots of the quadratic equation equal zero. The first solution was zero, while

the other two possible solutions were determined by the two conditions derived from the quadratic equation ($B^2 - 4AC = 0$ and $C = 0$) (Veksler and Gov, 2007; Kabaso et al., 2011b). The condition $B^2 - 4AC = 0$ yields the transition line of one additional solution (type I instability), and the condition $C = 0$ yields the transition line of two additional solutions (type II instability) (Fig. 5). The type I transition line was drawn in the phase diagram of the interplay between the spontaneous curvature of prominin nano-domains and the spontaneous curvature of I-BARs (Fig. 5(a) and (b)). The type I transition line determined the shift from stable to unstable regions, and therefore, for the sake of simplicity the type II transition line was not drawn. In this phase diagram analysis, the tube radius R was replaced by the value of 120 nm, which was also the equilibrium radius of the tubular structure given the abovementioned parameter values. Numerical solutions of the function of the phase diagram variables C_p and H_P were found.

According to the experimental results, the overexpression of I-BAR proteins can form a coat-like structure on the inner side of the membrane protrusion (Saarikangas et al., 2009). As a result, the elastic constant is predicted to increase considerably. In the following analysis, we evaluated the effects of high I-BAR density ($n = 1$) and high elastic constant ($\eta = 100$ kT) on tube stability for anisotropic and isotropic models (Fig. 5(c) and (d)). It was demonstrated that the scale of spontaneous curvatures of
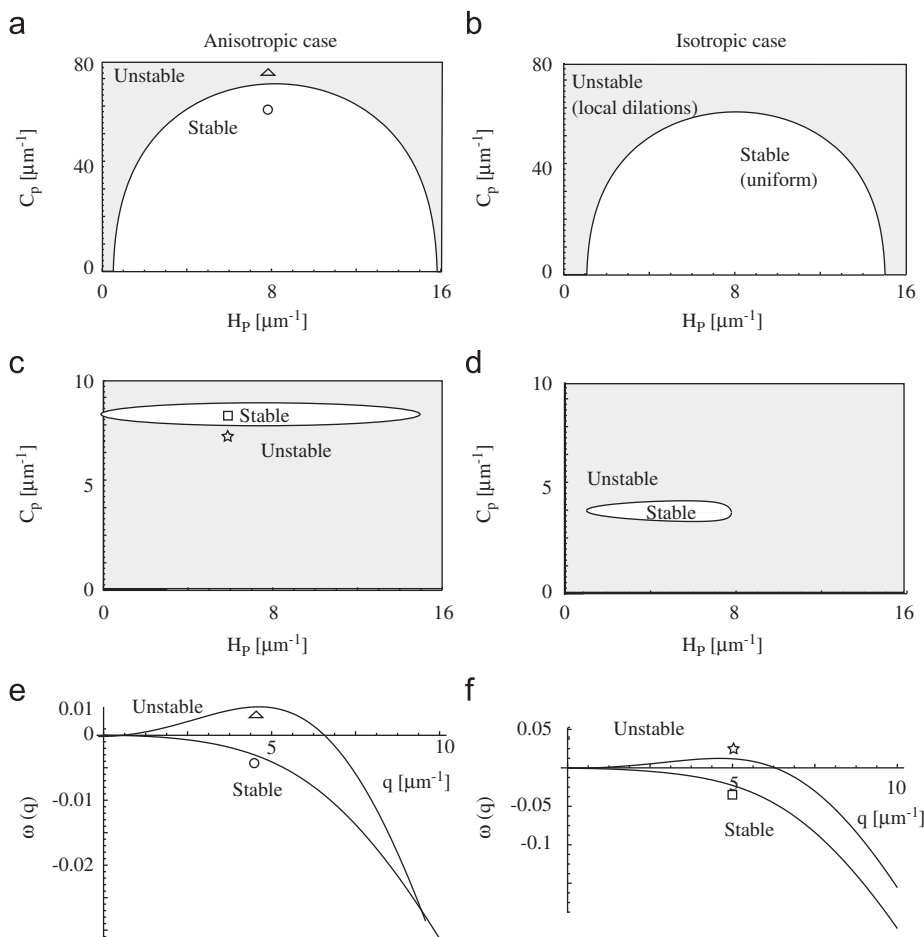
Fig. 5. The interplay between prominin nanodomains and I-BAR proteins on the stability of the membrane tube. Phase diagrams of the interplay between the spontaneous curvature of prominin nanodomain rafts (H_P) and the spontaneous curvature of I-BARs (C_p) for a membrane of anisotropic (a) and isotropic (b) elastic properties are shown. It is revealed that the anisotropic case has more stable regions than the isotropic one, and that the shift from stable to unstable regimes is through the type-I transition line. The effects of increasing the density (from $n = 0.1$ to $n = 1$) and the elastic constant (from $\eta = 1$ kT to $\eta = 100$ kT) of I-BAR proteins on the stability of the tubular membrane of anisotropic (c) and isotropic (d) elastic properties are shown for a membrane of anisotropic (c) and isotropic (d) elastic properties. Note the similar scale of H_P and C_p delineating the stable region. By increasing C_p, the dispersion relation of the system in (a) reveals a shift towards instability ($C_p = 60$ μm^{-1} ($\circ$), 80 μm^{-1} ($\triangle$)) (e). On the other hand, the system in (c) can also shift to instability by reducing C_p ($C_p = 8$ μm^{-1} ($\square$), 7 μm^{-1} ($\star$)) (f).

I-BARs and prominin rafts delineating the stable region is similar. More importantly, the size of the stable region is quite small, limiting the parameter space that allows a stable tube structure.

The stable and unstable regions in the phase diagram were confirmed in dispersion relations, where different values of C_P were incorporated (Fig. 5(e) and (f)). The effects of increasing the density (from $n = 0.1$ to $n = 1$) and the elastic constant (from $\eta = 1$ kT to $\eta = 100$ kT) of I-BAR proteins on tube stability were a narrowing of the parameter space of the stable region. Furthermore, the range of C_P and H_P delineating the stable region was similar.

5. Discussion

In the present study, an axisymmetric model of a membrane protrusion that included an inner membrane anisotropic component (i.e. prominin nanodomain rafts) and an outer membrane anisotropic component (i.e. attached I-BAR proteins), yet excluded actin filaments, was constructed. We investigated the underlying mechanisms contributing to the stability of the membrane protrusion (Fig. 2) and to irregularities in its diameter distribution (Fig. 3). The nearly homogeneous distribution of anisotropic prominin nanodomains along the membrane protrusion contributed to its stability (Fig. 2). The results of linear stability analysis of the membrane tubular shape showed that the equilibrium radius was mainly dependent on the spontaneous curvature of the anisotropic prominin rafts (Fig. 4). On increasing the flexural coefficient of I-BARs, the effects of I-BAR proteins on the equilibrium radius became considerable (Fig. 4). In addition, the membrane tube of anisotropic elastic properties was more stable and of smaller equilibrium radius than that calculated in the isotropic limit (Fig. 4). Using phase diagram analysis, we revealed an optimal range of values over which both prominin rafts and I-BAR proteins contributed to the tube stability (Fig. 5(a) and (b)). Increasing the density (from $n = 0.1$ to $n = 1$) and the elastic coefficient (from $\eta = 1$ kT to $\eta = 100$ kT) of I-BAR proteins considerably reduced the size of the stable region (Fig. 5(c) and (d)). The stable region was also denoted by spontaneous curvatures of I-BARs and prominin rafts of similar size.

According to the theory of isotropic membrane elasticity (Helfrich, 1973), the cell tubular membrane protrusion cannot be stabilized by isotropic membrane components alone (Miao et al., 1991; Derényi et al., 2002), but requires the accumulation of anisotropic membrane nanodomains (Iglič et al., 2006; Gimsa et al., 2007; Hurtig et al., 2010) (see also Fig. 4), or average orientational ordering of lipids (Kralj-Iglič et al., 2002). Therefore, the observed accumulation of anisotropic prominin nanodomain rafts could stabilize the highly curved membrane protrusion by overcoming the decrease in configurational entropy during the process of lateral sorting of the membrane components (Kralj-Iglič et al., 1999; Iglič et al., 2006). These theoretical studies provide insight into the stability of the tubular membrane protrusion following the disassembly of the inner rod cytoskeleton (Veranič et al., 2008), or into the stability of actin-free filopodia (Yang et al., 2009).

Generally, the polymerization of actin filaments was considered to be the main force responsible for the formation of the membrane protrusion. However, a recent study revealed that actin filaments were not present in all filopodia, and that the polymerization of actin filaments lags behind the accumulation of I-BAR proteins at the tip of filopodia (Yang et al., 2009). This suggests that I-BAR proteins may have an important role in the protrusive force. In addition, the formation of helical coat of I-BAR proteins (Yang et al., 2009) underneath the membrane would also suggest their role in promoting stability (Heinrich et al., 2010). The observed irregularities in the shape of actin-free membrane tubes could be partially due to changes in the density distribution of I-BAR proteins (Figs. 3 and 5), while the role of actin filaments

could be to establish long-term stability and to facilitate retrograde transport of molecules. Here it was demonstrated that coupling between the spontaneous curvature of I-BAR proteins and the membrane curvature could lead to dynamic instability, suggesting the aggregation of I-BAR proteins at the tip of membrane protrusions.

According to their X-ray crystallographic structures and the overexpression of BAR domains in GUVs, it has been shown that the spontaneous curvature range of BAR proteins is approximately between 30 and 80 μm^{-1} (Shimada et al., 2007; Saarikangas et al., 2009). Since the spontaneous curvature radius of I-BAR proteins is on the same scale as their length, the spontaneous curvature of prominin nanodomain rafts could be one order of magnitude smaller than the spontaneous curvature of I-BAR proteins. We here report that the range of spontaneous curvature of prominin nanodomain rafts and I-BAR proteins is within the range described in the phase diagram (Fig. 5). In fact, the proposed spontaneous curvatures of prominin rafts and I-BARs put the system near the transition line from stability to instability, such that changes in the density of I-BAR proteins could drive dynamic instability leading to contraction of the tube (Figs. 3 and 5). A future study should investigate this dynamic instability, modelling the curvature dependent fluxes of I-BAR proteins along the tube and towards the tip of the membrane protrusion.

The results and conclusions of the present study are applicable to other experimental systems of tubular membrane structures, consisting of stabilizing (stationary) and destabilizing (mobile) membrane components. On a final note, elucidating the basic mechanisms contributing to the stability of highly curved tubular structures such as tubular membrane protrusions could provide insight into basic mechanisms related to cell shaping, cell growth and cell motility.

Conflict of interest statement

There were no conflicts of interest regarding this work.

Acknowledgements

Appendix A. Supplementary data

Supplementary data associated with this article can be found in the online version at doi:10.1016/j.jbiomech.2011.10.039.

References

Baumgart, T., Capraro, B.R., Zhu, C., Das, S.L., 2011. Thermodynamics and mechanics of membrane curvature generation and sensing by proteins and lipids. Annual Review of Physical Chemistry 62, 483–506.

Corbeil, D., Röper, K., Fargeas, C.A., Joester, A., Huttner, W.B., 2001. Prominin: a story of cholesterol, plasma membrane protrusions and human pathology. Traffic 2, 82–91.

Davis, D.M., Sowinski, S., 2008. Membrane nanotubes: dynamic long-distance connections between animal cells. Nature Reviews Molecular Cell Biology 6, 431–436.

Derényi, I., Jülicher, F., Prost, J., 2002. Formation and interaction of membrane tubes. Physical Review Letters 88, 238101.

Dubey, G.P., Ben-Yehuda, S., 2011. Intercellular nanotubes mediate bacterial communication. Cell 144, 590–600.

Fischer, T., 1992. Bending stiffness of lipid bilayers. III. Gaussian curvature. Journal de Physique II (France) 2, 337–343.

Fošnarič, M., Iglič, A., May, S., 2006. Influence of rigid inclusions on the bending elasticity of a lipid membrane. Physical Review E 174, 051503.

Gerdes, H.H., Bukoreshtiev, N.V., Barroso, J.F.V., 2007. Tunneling nanotubes: a new route for the exchange of components between animal cells. FEBS Letters 581, 2194–2201.

Gimsa, U., Iglič, A., Fiedler, S., Zwanzig, M., Kralj-Iglič, V.L., Jonas, L., Gimsa, J., 2007. Actin is not required for nanotubular protrusions of primary astrocytes grown on metal nano-lawn. Molecular Membrane Biology 24, 243–255.

Góźdź, W.T., 2004. Spontaneous curvature induced shape transformations of tubular polymersomes. Langmuir 20, 7385–7391.

Góźdź, W.T., 2005. Influence of spontaneous curvature and microtubules on the conformations of lipid vesicles. The Journal of Physical Chemistry B 109, 21145–21149.

Góźdź, W.T., 2006. The interface width of separated two-component lipid membranes. Journal of Physical Chemistry B 110, 21981–21986.

Góźdź, W.T., 2011. Shape transformation of lipid vesicles induced by diffusing macromolecules. Journal of Chemical Physics 134, 024110.

Heath, R.J.W., Install, R.H., 2008. F-BAR domains: multifunctional regulators of membrane curvature. Journal of Cell Science 121, 1951–1954.

Heinrich, M.C., Capraro, B.R., Tian, A., Isas, J.M., Langen, R., Baumgart, T., 2010. Quantifying membrane curvature generation of *Drosophila* amphiphysin N-BAR domains. The Journal of Physical Chemistry Letters 1, 3401–3406.

Helfrich, W., 1973. Elastic properties of lipid bilayers: theory and possible experiments. Zeitschrift für Naturforschung C 28, 693–703.

Hurtig, J., Chiu, T., Onfelt, B., 2010. Intercellular nanotubes: insights from imaging studies and beyond. Wiley Interdisciplinary Reviews: Nanomedicine and Nanobiotechnology 2, 260–276.

Huttner, H.B., Zimmerberg, J., 2001. Implications of lipid microdomains for membrane curvature, budding and fission. Commentary Current Opinion Cell Biology 13, 478–484.

Iglič, A., Babnik, B., Gimsa, U., Kralj-Iglič, V., 2005. On the role of membrane anisotropy in the beading transition of undulated tubular membrane structures. Journal of Physics A: Mathematical and General 38, 8527–8536.

Iglič, A., Hägerstrand, H., Veranič, P., Plemenitaš, V., Kralj-Iglič, V., 2006. Curvature induced accumulation of anisotropic membrane components 29 and raft formation in cylindrical membrane protrusions. Journal of Theoretical Biology 240, 368–373.

Iglič, A., Babnik, B., Fošnarič, M., Hägerstrand, H., Kralj-Iglič, V., 2007a. On the role of anisotropy of membrane constituents in formation of a membrane neck during budding of multicomponent membrane. Journal of Biomechanics 40, 579–585.

Iglič, A., Lokar, M., Babnik, B., Slivnik, T., Veranič, P., Hägerstrand, H., Kralj-Iglivč, V., 2007b. Possible role of flexible red blood cell membrane nanodomains in the growth and stability of membrane nanotubes. Blood Cells, Molecules and Diseases 39, 14–23.

Itoh, T., Erdmann, K.S., Roux, A., Habermann, B., Werner, H., De Camilli, P., 2005. Dynamin and the actin cytoskeleton cooperatively regulate plasma membrane invagination by BAR and F-BAR proteins. Developmental Cell 23, 791–804.

Janich, P., Corbeil, D., 2007. GM1 and GM3 lipids highlight distinct lipid microdomains with the apical domain of epithelial cells. FEBS Letters 581, 1783–1787.

Jorgačevski, J., Fošnarič, M., Vardjan, N., Stenovec, M., Potokar, M., Kreft, M., Kralj-Iglič, V., Iglič, A., Zorec, R., 2010. Fusion pore stability of peptidergic vesicles. Molecular Membrane Biology 27, 65–80.

Kabaso, D., Shlomovitz, R., Auth, T., Lew, V.L., Gov, N.S., 2010. Curling and local shape changes of red blood cell membranes driven by cytoskeletal reorganization. Biophysical Journal 99, 808–816.

Kabaso, D., Shlomovitz, R., Schloen, K., Stradal, T., Gov, N.S., 2011a. Theoretical model for cellular shapes driven by protrusive and adhesive forces. PLoS Computational Biology 7, 1–13.

Kabaso, D., Gongadze, E., Elter, P., van Rienen, K.U., Gimsa, J., Iglič, A., 2011b. Attachment of rod-like (BAR) and membrane shape. Mini-Reviews in Medicinal Chemistry 11, 272–282.

Kralj-Iglič, V., Heinrich, V., Svetina, S., Zeks, B., 1999. Free energy of closed membrane with anisotropic inclusions. The European Physical Journal B 10, 5–8.

Kralj-Iglič, V., Iglič, A., Gomišček, G., Sevšek, F., Arrigler, V., Hägerstrand, H., 2002. Microtubes and nanotubes of a phospholipid bilayer membrane. Journal of Physics A: Mathematical and General 35, 1533–1549.

Lokar, M., Iglič, A., Veranič, P., 2010. Protruding membrane nanotubes: attachement of tubular protrusions to adajacent cells by several anchoring junctions. Protoplasma 246, 81–87.

Mattila, P.K., Pykalainen, A., Saarikangas, J., Paavilainen, V.O., Vihinen, H., Jokitalo, E., Lappalainen, P., 2007. Missing-in-metastasis and IRSp53 deform PI(4,5)P2-rich membranes by an inverse BAR domain-like mechanism. Journal of Cell Biology 176, 953–964.

Miao, L., Fourcade, B., Rao, M., Wortis, M., Zia, R.K.P., 1991. Equilibrium budding and vesiculation in the curvature model of fluid lipid vesicles. Physical Review E 43, 6843–6856.

Millard, T.H., Bompard, G., Heung, M.Y., Dafforn, T.R., Scott, D.J., Machesky, L.M., Futterer, K., 2005. Structural basis of Filopodia formation induced by the IRSp53/MIM homology domain of human IRSp53. The EMBO Journal 24, 240–250.

Perutkova, Š., Kralj-Iglič, V., Frank, M., Iglič, A., 2010. Mechanical stability of membrane nanotubular protrusions influenced by attachment of flexible rod-like proteins. Journal of Biomechanics 43, 1612–1617.

Risselada, H.J., Marrink, S.J., Müller, M., 2011. Curvature-dependent elastic properties of liquid-ordered domains result in inverted domain sorting on uniaxially compressed vesicles. Physical Review Letters 106, 148102.

Rituper, B., Davletov, B., Zorec, R., 2010. Lipid–protein interactions in exocytotic release of hormones and neurotransmitters. Clinical Lipidology 5, 747–761.

Röper, K., Corbeil, D., Huttner, W.B., 2000. Retention of prominin in microvilli reveals distinct cholesterol-based lipid microdomains in the apical plasma membrane. Nature Cell Biology 2, 582–592.

Rustom, A., Saffrich, R., Markovic, I., Walther, P., Gerdes, H., 2004. Nanotubular highways for intercellular organelle transport. Science 303, 1007–1010.

Saarikangas, J., Zhao, H., Pykäläinen, A., Laurinmäki, P., Mattila, P.K., Kinnunen, P.K., Butcher, S.J., Lappalainen, P., 2009. Molecular mechanisms of membrane deformation by I-BAR domain proteins. Current Biology 19, 95–107.

Scita, G., Confalonieri, S., Lappalainen, P., Suetsugu, S., 2008. Irsp53: crossing the road of membrane and actin dynamics in the formation of membrane protrusions. Trends in Cell Biology 18, 52–60.

Shimada, A., Niwa, H., Tsujita, K., Suetsugu, S., Nitta, K., et al., 2007. Curved EFC/F-BAR-domain dimers are joined end to end into a filament for membrane invagination in endocytosis. Cell 129, 761–772.

Shlomovitz, R., Gov, N.S., 2008. Physical model of contractile ring initiation in dividing cells. Biophysical Journal 94, 1155–1168.

Sorre, B., Callan-Jones, A., Manneville, J.B., Nassoy, P., Joanny, J.-F., Prost, J., Goud, B., Bassereau, P., 2009. Curvature-driven lipid sorting needs proximity to a demixing point and is aided by proteins. Proceedings of the National Academy of Sciences of the United States of America 106, 5622–5626.

Tian, A., Baumgart, T., 2009. Sorting of lipids and proteins in membrane curvature gradients. Biophysical Journal 96, 2676–2688.

Veksler, A., Gov, N.S., 2007. Phase transitions of the coupled membrane–cytoskeleton modify cellular shape. Biophysical Journal 93, 3798–3810.

Veranič, P., Lokar, M., Schuetz, G.J., Weghuber, J., Wieser, S., Hagerstrand, H., Kralj-Iglič, V., Iglič, A., 2008. Different types of cell-to-cell connections mediated by nanotubular structures. Biophysical Journal 95, 4416–4425.

Weigmann, A., Corbeil, D., Hellwig, A., Huttner, W.B., 1997. Prominin, a novel microvilli-specific polytopic membrane protein of the apical surface of epithelial cells, is targeted to plasmalemmal protrusions of non-epithelial cells. Proceedings of the National Academy of Sciences of the United States of America 74, 12425–12430.

Yang, C., Hoelzle, M., Disanza, A., Scita, G., Svitkina, T., 2009. Coordination of membrane and actin cytoskeleton dynamics during filopodia protrusion. PLoS One 4, e5678.

Zhao, H., Pykäläinen, A., Lappalainen, P., 2010. I-BAR domain proteins: linking actin and plasma membrane dynamics. Current Opinion in Cell Biology 23, 1–8.